Mass Estimation Through Fusion of Astrometric and Photometric Data Collection with Applications to Orbital Debris Characterization[1]

Matthew Richardson and Tom Kelecy
L3 Applied Defense Solutions

ABSTRACT

A formulation is presented for estimating the mass of a space object from the fusion of astrometric and photometric data. The application for such a tool is to characterize the mass of an unknown debris object and quantify the mass uncertainty through the estimation method. Typically, the orbit dynamics are observed with angles measurements to deduce area-to-mass ratio. Photometric data is not sensitive to mass but is a function of the albedo-area and attitude dynamics of the space object. Thus, from these two data types it is possible to disentangle intrinsic properties using albedo-area and area-to-mass and ultimately determine the mass of a space object. Two case studies were analyzed using a 3-axis stabilized, operational geosynchronous satellite and a debris high area-to-mass ratio object. Simulated data was processed through an unscented Schmidt-Kalman filter to estimate the translational and rotational states of the space object as well as the mass. In both cases analyzed the filter was able to accurately converge on the true mass of the given space object to within 5% uncertainty. This will facilitate understanding of unknown debris objects when characterizing such objects with quantifiable uncertainty. Observability of the states was examined and shown, when relevant, to be a good indicator of when mass, size and attitude can be estimated.

1. INTRODUCTION

Previous research has demonstrated the viability of estimating mass of resident space objects (RSO) [8, 9, 30]. These all leverage the "physics" associated with perturbations in the astrometric tracking data due to solar radiation pressure which provides information on the area-to-mass ratio attribute, and the reflected light, or photometric magnitude, which relates the size attribute. By combining the area-to-mass ratio and size estimates an estimate of the mass can be derived. Accurate estimation of mass is problematic in the absence of specific details on the size, shape and attitude, in addition to the reflective attributes, in particular in the case of unknown space debris. In this work we are attempting to take steps towards a "practical" implementation which accounts for uncertainty, or lack of exact knowledge, of certain physical attributes (e.g. size, attitude, etc.) through a consider covariance implementation (namely the unscented Schmidt-Kalman Filter, USKF). We are also attempting to gain insight into when we can or cannot estimate relevant parameters through use of the Fisher information (observability). In this paper, we present work that demonstrates how these tools can be used to gain more confidence in estimated mass and its uncertainty which may inform the data collection and estimation strategy as we move towards processing real data on remote space debris objects.

2. METHODS AND BACKGROUND

1.1 Mass Estimation Methods

Commonly, mass is determined indirectly using the effective albedo area-to-mass ratio that comes out of current orbit determination processes. This value is based on solar radiation pressure. That value is then divided by a corresponding albedo area that is based on photometry [8, 9]. Due to dynamic mismodeling of space objects this can sometimes lead to inconsistent predictive results. The issue for mass estimation methods is to accurately fuse astrometric data and photometric data together to extract where each has its strengths.

The angles measurements are very sensitive to the effective albedo area-to-mass ratio when it comes to solar radiation pressure while the photometry is sensitive to the effective observed from a specific sensor site. These two quantities are only the same at zero phase angle, i.e. the sun is directly behind the observer. An example of this is illustrated in the Figure. 1:

1 Continuation of work from Masters Thesis completed at California Polytechnic State University, San Luis Obispo: http://digitalcommons.calpoly.edu/theses/1742/

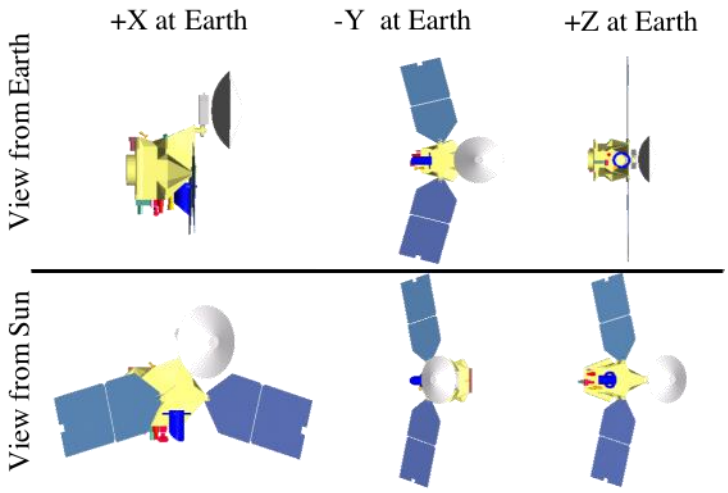

Figure 1. Observer vs. Sun Views of Hypothetical Satellite

It is evident that the area which is facing an observer will be different than the side exposed to the incident flux of the Sun. Thus, the albedo-area value that is observable from the optical site (i.e. associated with photometric brightness) will be different than the albedo value from the point of view of the sun (i.e. associated with astrometric-determined solar radiation pressure) and is heavily dependent on the object's attitude.

This topic has importance to the orbital space community for characterizing unknown spacecraft and debris. In particular for debris, High Area to Mass Ratio (HAMR) objects have a very unpredictable nature. Methods of initial orbit determination need a survey of multiple nights worth of consistent data to stitch together a hypothesized orbit track for a certain space object [27, 30]. Due to the significant effect of solar radiation pressure on these HAMR object's eccentricities and inclinations, they can be within a field of view one night and perturbed out of the field of view by the next observing time frame. Thus, it is important to identify and characterize these objects within as short of a period of time as possible as to not lose track of them. Enhanced tracking and characterization of HAMR objects will allow further information to be gained about this class of space debris. This, in turn, will provide further information into the origin and dynamics of other similar space objects.

HAMR objects are a particularly important set of space objects to study because they can pose collision hazards with GEO objects due to their large variations in eccentricity and inclination, as well as their difficult-to-predict trajectory. Unfortunately, their intrinsic characteristics are unknown except for the properties for which they got their name. Their area-to-mass ratios, $\frac{C_r A}{m}$, can range anywhere from 0.1 to 20 m^2/kg [27] as compared to typical area-to-mass ratio values of 0.001-0.05 m^2/kg for operational satellites. HAMR objects are prone to solar radiation pressure (SRP) on a much more significant scale than any other object in their locality. This poses a challenge for consistent tracking leading to the cataloguing of such objects. A site might serendipitously observe a HAMR object, but identification and association of follow up tracks prove to be non-trivial due to the significant perturbation effects combined with their dim apparent time-varying reflective light intensity magnitudes. HAMR objects have difficult to predict orbit tracks that can cause potential collision hazards with the active GEO population. Thus, in order to create a reliable catalogue of the HAMR object population, it is important to accurately deduce intrinsic characteristics such as area, albedo, and mass.

1.2 Background

Astrometric, or angles data, originates from a sensor (typically a telescope) that takes pictures of the night sky over a certain period of time. A reduction process is conducted to determine the location of the streak in the night sky through comparison of known stars and thereby computing the angular information. Photometric data, or light information coming from a charge-coupled-device camera (CCD), observes magnitude and direction of a particular light source, which gives information on the space object. The challenge when applying this to HAMR objects, as discussed previously, is that astrometric data gives you positional information and, hence, perturbations on the

orbital dynamics that are only indirectly related to the photometric signature. The photometric signatures give you attitude related information which effects the positional perturbations. An investigation into coupling the strengths of each data type to determine characteristics such as mass and when the quantities are observable is the primary focus of this work.

Gauss iteration is an angles only solution to initial orbit determination that uses three different observations as a method to formulate a position and velocity vector for a space object. The formulation derives a line of sight vector by the right ascension and declination values, a site vector described using the local sidereal time of each observation, and the time difference between each observation. Gauss' method was chosen in comparison to the other IOD methods, such as double-r or Izzo-Gooding [23], because it is better at handling objects which do not have a lot of angular separation. This made it ideal for the purposes of this work due to the short data collection time window of HAMR objects in orbit and the GEO regime in which the objects reside. However, it is important to be aware of the limitations of Gauss' method such as its sensitivity to data noise and inefficiency with collections spanning more than 60° [23].

It has been shown in [27] that angles data can produce information about an area-to-mass ratio due to SRP forces. However, that study was restricted in terms of rotational dynamic modeling. When combined with the typically dim magnitudes of HAMR objects, the result was lost or incorrectly associated space objects. To accurately estimate the translational and rotational dynamics of a known object data must be consistently taken over a span of multiple days for that same object. Unfortunately, this is not feasible for something like a HAMR object since the drastic changes in eccentricity and inclination can perturb the object out of a known orbit track within a period of a few hours. With the attempt of infusing the UKF with periodic photometric measurements, mass properties should be more accurately modeled.

Light curves are able to estimate the shape and albedo properties of a space object. Kaasalainen and Torppa [29] were able to deduce the rotation period, pole direction, and scattering parameters of an asteroid using only light curve information. Since magnitude information can also be used to deduce information about position and attitude and their respective rates [24] utilizing photometric information can be considerably useful in determining mass information for a space object. This is because there are multiple ways to approach the modeling information of intrinsic parameters which are all not sensitive to the same restrictions. Thus, when incorporated in conjunction, astrometric and photometric data can each provide useful characteristics to deduce mass.

3. UNSCENTED SCHMIDT KALMAN FILTER IMPLEMENTATION

3.1 Force and Torque Model Development

3.1.1 Shape Model

A simple rectangular prism was used as the shape model in this study. The finite number of flat facets, six in the case of the rectangular prism, allowed for information to be propagated through the experimentation as the object was allowed to rotate. Each facet had a set of three basis vectors to parametrize the surface $\langle \mathrm{u}_u^B, \mathrm{u}_v^B, \mathrm{u}_n^B \rangle$ where u_u^B and u_v^B were in the plane of the facet and u_n^B was normal to the facet. Because the space object was considered to be a rigid body, the unit basis vectors did not change with time with respect to the body frame of reference.

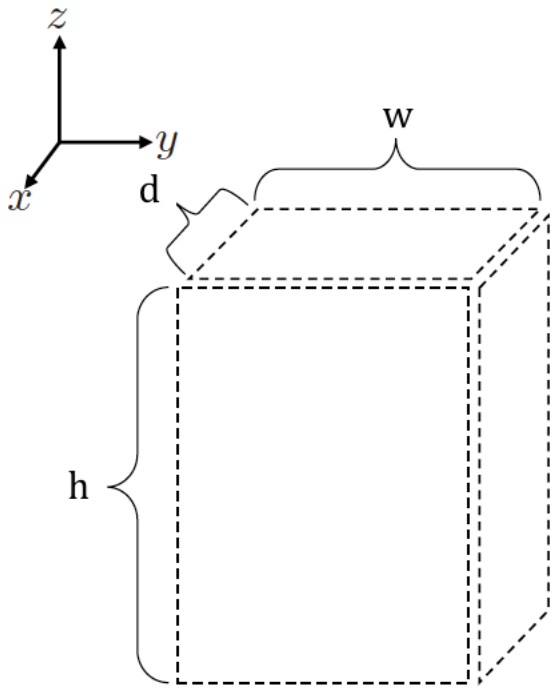

Figure 2. Rectangular Prism Shape Model

The SRP and light curve models require these vectors to be expressed in the inertial coordinate system. To do so, accounting for the rotational dynamics of the space object, we can map the body reference frame to the inertial reference frame using an attitude matrix $A(\boldsymbol{\varrho}_I^B)$ given by

$$\mathrm{u}_k^B = A(\boldsymbol{\varrho}_I^B)\mathrm{u}_k^I, \quad k = u, v, n$$

where $\boldsymbol{\varrho}_I^B$ is the quaternion of the state. The six sides of the rectangular prism space object each had a surface facet unit normal to keep track of when the object was rotating in the inertial frame. The area vector A has dimension n by 1 where n is the number of facets the object has. This vector was propagated alongside the equations of motion but should remain unchanged as the object orbits on account of the assumption of a rigid body.

3.1.2 Solar Radiation Pressure

For objects orbiting at high altitudes ≥ 1,000 km the dominating non-gravitational perturbation force is solar radiation pressure (SRP). To accurately describe the effects SRP has on a space object, position and attitude dynamics must be coupled together. Additionally, parameters such as reflectivity and the solar flux arriving at the space object's position (accounting for shadowing effects) must be correctly determined. This work assumes a constant average flux coming from the Sun at all periods where in all reality this simplification would not be true for periods of intense solar activity, when the value would be much larger or conversely in periods of low activity when the effect might be negligible. Because the incoming radiation from the Sun exerts a force on the space object, the apparent size of the space object that faces the Sun is critical in accurately determining the amount of acceleration. According to Vallado and McClain [23], the force can be modeled as

$$\mathbf{F}_{srp} = -p_{srp} c_R A_{\odot} \frac{\mathbf{r}_{so\odot}}{r_{so\odot}}$$

where p_{srp} is the pressure due to solar radiation, c_R is the coefficient of reflectivity, $A_\odot$ is the exposed area to the Sun, and $\mathbf{r}_{so\odot}$ is the position vector from the space object to the Sun. In this case the average solar pressure is modeled by

$$p_{srp} = \frac{\Phi_{sun}}{c} = \frac{1467}{3 \times 10^8} \frac{W/m^2}{m/s} = 4.57 \times 10^{-}6 \frac{N}{m^2}$$

acceleration is obtained by using Newton's second law with the given force

$$a_{srp} = \frac{F_{srp}}{m} = \frac{-p_{srp} c_R A_\odot}{m}$$

Due to the material property of a space object, some sides will reflect diffusely while others will reflect specularly. Hence, at any moment the space object will experience a net force plus a net torque. Considering this, the angle at which the solar radiation is incident on a surface element of area $A_\odot$, whose surface normal vector makes a solar-incident angle ϕ_{inc} with the Sun-space object line. In assuming the diffuse and specular radiation forces are Lambertian diffusion and mirror-like specular reflection, DeMars [28] derives the acceleration due to solar radiation pressure acting on a body composed of n flat plates as

$$\mathbf{a}^i_{srp} = -p_{srp} (\frac{r_{au}}{r_{so}})^2 \sum_{k=1}^{n} \quad \frac{A_k}{m} cos\phi_k [(1 - \rho_k)\mathbf{u}^I_{sun} + 2(\frac{1}{3}\delta_k + cos\phi_k \rho_k)\mathbf{u}^I_{n,k}]$$

where r_{au} is the distance of one astronomical unit, $r_{so} = \|\mathbf{r}^I_{sun} - \mathbf{r}^I\|$ is the distance of the Sun with respect to the space object, m is the total space object mass, A_k is the area of the k^{th} plate, ρ_k is the specular reflection coefficient of the k^{th}plate, δ_k is the diffuse reflection coefficient of the k^{th} plate, $\mathbf{u}^I_{n,k}$ is the unit vector normal to the k^{th} plate expressed in the inertial frame. The solar-incident angle ϕ_k is given by

$$cos\phi_k = \mathbf{u}^I_{n,k} \cdot \mathbf{u}^I_{sun}$$

where $\mathbf{u}^I_{sun}$ is the unit vector space object to the Sun expressed in the inertial reference frame, which is given by

$$\mathbf{u}^I_{sun} = \frac{\mathbf{r}^I_{sun} - \mathbf{r}^I}{\|\mathbf{r}^I_{sun} - \mathbf{r}^I\|}$$

3.2 Observation Models

3.2.1 Photometric Model

The optical site records position of the space object as well as the magnitude of the brightness. That brightness can be modeled using a bidirectional reflectance distribution function (BRDF) which is a way to model light scattered from the surface of an object due to incident light. The BRDF at any point on the surface is a function of two directions: the direction from which the light source originates and the direction from which the scatter light leaves the surface [24]. Thus, the total BRDF is a sum of a specular and a diffuse component given by

$$\rho_{total}(i) = \rho_{spec}(i) + \rho_{diff}(i)$$

The diffuse component is Lambertian diffusion, scattering the light equally in all directions while the specular component are the mirror-like characteristics, concentrating the light in one particular location. Ashikhmin and Shirley [25] develops a BRDF for modeling continuous arbitrary surfaces but simplifies it for flat surfaces. This can then be applied to the n sided flat surface model employed in this work. Under this flat plate simplification [25]

$$\rho_{spec}(i) = C_{spec}\frac{(\mathbf{u}_{obs}\cdot\mathbf{u}_{spec})^{\alpha}}{\mathbf{u}_{sun}\cdot\mathbf{u}_{n}},$$

where $\mathbf{u}_{spec} = 2(\mathbf{u}_n\cdot\mathbf{u}_{sun})\mathbf{u}_n - \mathbf{u}_{sun}$ and is the unit vector in the direction of specular reflection, C_{spec} is the coefficient of specular reflectivity, and α defines the width of the specular lobe, $\mathbf{u}_n^I(i)$ is the unit normal of the i^{th} plate, and $\mathbf{u}_{sun}$ is the unit vector of the Sun's direction. Then the diffuse component is given by

$$\rho_{diff}(i) = \frac{C_{diff}}{\pi}$$

where C_{diff} is the coefficient of diffuse reflectivity. Knowing this the flux equations can be developed. The flux of visible light which reaches the surface of the space object is modeled by

$$F_{sun}(i) = \Phi_{sun,vis}\rho_{total}(i)(\mathbf{u}_n^I(i)\cdot\mathbf{u}_{sun}^I)$$

where $\Phi_{sun,vis} = 455\ W/m\text{^}2$ is the average power per square meter from the sun striking the surface of the object and the unit vectors are as previously defined. Keeping in mind that if for any side the angle between the surface normal and the Sun's direction was larger than $\pi/2$, than the solar flux would be set to zero since there was no radiant flux on that facet. Then the reflected light becomes

$$F_{obs}(i) = \frac{F_{sun}(i)A(i)(\mathbf{u}_n^I(i)\cdot\mathbf{u}_{sun}^I)}{\|\mathbf{d}^I\|^2}$$

where $A(i)$ is the area of the i^{th} facet and the other terms are as previously defined. Finally, the apparent magnitude can be calculated as

$$m_{app} = -26.7 - 2.5log_{10}|\sum_{i=1}^{n}\frac{F_{obs}(i)}{\Phi_{sun,vis}}|$$

where -26.7 is the apparent magnitude of the Sun.

3.2.2 Earth Shadow Calculation

The solar radiation model and observation model were equipped with the ability to handle shadow calculations for when a spacecraft is passing in the shadow of the Earth such as can be seen in Figure 3. To do so, the translational and rotational model considers the current position vector of the space object and the current position vector of the Sun. The angle between the two objects with the common central body of Earth can be found using

$$\theta = cos^{-1}(\frac{\mathbf{r}_{\odot}\cdot\mathbf{r}_{so}}{r_{\odot}r_{so}})$$

where $\mathbf{r}_{\odot}$ is the position vector of the Sun, $\mathbf{r}_{so}$ is the position vector of the space object, $r_{\odot} = \|\mathbf{r}_{\odot}\|$, and $r_{sc} = \|\mathbf{r}_{sc}\|$,. Then each object makes a tangent line with the edge of Earth, which forms a triangle with vertex angle given by

$$\theta_{so} = cos^{-1}(\frac{R_{\oplus}}{r_{so}}) \quad \theta_{\odot} = cos^{-1}(\frac{R_{\oplus}}{r_{\odot}})$$

where $R_{\oplus}$ is the radius of the Earth, meaning that there is no line of site between the space object and the sun when $\theta_{so} + \theta_{\odot} < \theta$ [26]. Each unit normal vector of the facet was constantly checked with the vector position of the sun. If the addition of the two angles were greater than the sum of the angle between them then SRP and measurement fluxes were set to zero.

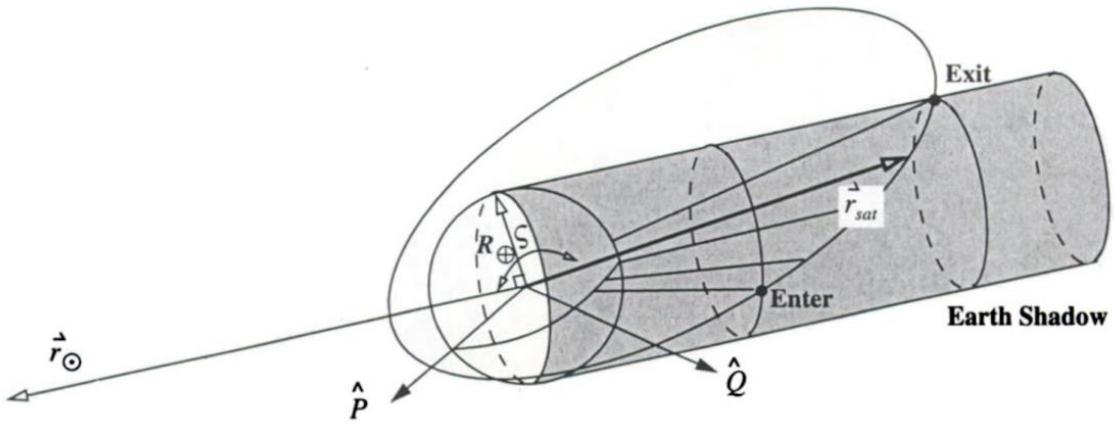

Figure 3. Shadow Model

Reference [27] shows that using a simple cylindrical Earth shadow model can result in errors in the force modeling. These errors should be accounted for in future work if attempting to obtain the highest accuracy for the orbit kinematics.

Because the dynamics of this model are in terms of the body coordinate system, this model needs to keep track of the orientation of the space object with respect to the inertial frame. To do so, every iteration of the function takes in the unit body frame vectors and translates it into the inertial frame using the direction cosine matrix (DCM) which can be constructed from the quaternion in the current state vector. The body coordinate unit vectors are divided by the attitude matrix to produce unit normal vectors. The inertial unit vectors are also used to keep track of which facet of the rectangular prism was facing towards the sun and which of those are not at every time instance. If for any side the angle between the surface normal and the Sun's direction is larger than $\pi/2$, than the solar radiation pressure is set to zero since there was no radiant flux on that facet.

3.3 Unscented Schmidt-Kalman Filter

As mentioned previously, in order to account for, or "consider", the uncertainty associated with non-estimated parameters, the unscented Schmidt-Kalman filter (USKF) is utilized. Using by-products of the USKF algorithm, the Fisher information can be computed, giving a measure of the observability of estimated parameters, mass being the parameter of interest here. The USKF is implemented in The Infinity Filter construct.

Stauch and Jah [31] presented the USKF. There are two general categories of consider techniques. One is consider analysis, in which a typical state filter is executed and after the measurement update, the uncertainties of the consider parameters are mapped into the state. The other is a consider filter, in which the state itself is augmented with the consider parameters, but the consider parameter value and uncertainty are forced to be unchanged. Thus, the consider parameters are directly included in the filtering process. The USKF algorithm is given in Table 1, alongside the unscented Kalman Filter (UKF) algorithm.

	UKF	USKF
Predictive	$\mathbf{S}_{k-1} = Cholesky(\mathbf{P}_{k-1})$ $\boldsymbol{X}_{i,k-1} = \hat{\boldsymbol{x}}_{k-1} \pm \sqrt{n_x}\boldsymbol{s}_{i,k-1}$ where $\mathbf{S} = [\boldsymbol{s}_1, \boldsymbol{s}_2, ..., \boldsymbol{s}_{n_x}]$ $w = \frac{1}{2n_x}$ $\boldsymbol{X}_{i,k} \Leftarrow \dot{\boldsymbol{X}}_i = \boldsymbol{f}(\boldsymbol{X}_{i,k-1}, t)$ $\hat{\boldsymbol{x}}_k = \sum_{i=1}^{2n_x} w_i \boldsymbol{X}_{i,k}$ $\mathbf{P}_k = \sum_{i=1}^{2n_x} w_i (\boldsymbol{X}_{i,k} - \hat{\boldsymbol{x}}_k)(\boldsymbol{X}_{i,k} - \hat{\boldsymbol{x}}_k)^T$	$\mathbf{S}_{zz,k-1} = Cholesky(\mathbf{P}_{\boldsymbol{zz},k-1})$ $\boldsymbol{Z}_{i,k-1} = \hat{\boldsymbol{z}}_{k-1} \pm \sqrt{n_x + n_c}\boldsymbol{s}_{i,k-1}$ where $\mathbf{S}_{zz} = [\boldsymbol{s}_1, ..., \boldsymbol{s}_{n_x+n_c}]$ $w = \frac{1}{2(n_x+n_c)}$ $\boldsymbol{Z}_{i,k} \Leftarrow \dot{\boldsymbol{Z}}_i = \boldsymbol{f}(\boldsymbol{Z}_{i,k-1}, t)$ $\hat{\boldsymbol{z}}_k = \sum_{i=1}^{2(n_x+n_c)} w_i \boldsymbol{Z}_{i,k}$ $\mathbf{P}_{\boldsymbol{zz},k} = \sum_{i=1}^{2(n_x+n_c)} w_i (\boldsymbol{Z}_{i,k} - \hat{\boldsymbol{z}}_k)(\boldsymbol{Z}_{i,k} - \hat{\boldsymbol{z}}_k)^T$
Corrective	$\boldsymbol{Y}_i = \boldsymbol{h}(\boldsymbol{X}_i, t)$ $\hat{\boldsymbol{y}} = \sum_{i=1}^{2n_x} w_i \boldsymbol{Y}_i$ $\mathbf{P}_{\boldsymbol{yy}} = \sum_{i=1}^{2n_x} w_i (\boldsymbol{Y}_i - \hat{\boldsymbol{y}})(\boldsymbol{Y}_i - \hat{\boldsymbol{y}})^T + \boldsymbol{R}$ $\mathbf{P}_{\boldsymbol{xy}} = \sum_{i=1}^{2n_x} w_i (\boldsymbol{X}_i - \hat{\boldsymbol{x}})(\boldsymbol{Y}_i - \hat{\boldsymbol{y}})^T$ $\mathbf{K} = \mathbf{P}_{\boldsymbol{xy}}\mathbf{P}_{\boldsymbol{yy}}^{-1}$ $\hat{\boldsymbol{x}}^+ = \hat{\boldsymbol{x}}^- + \mathbf{K}(\boldsymbol{y} - \hat{\boldsymbol{y}})$ $\mathbf{P}^+ = \mathbf{P}^- - \mathbf{K}\mathbf{P}_{\boldsymbol{yy}}\mathbf{K}^T$	$\boldsymbol{Y}_i = \boldsymbol{h}(\boldsymbol{Z}_i, t)$ $\hat{\boldsymbol{y}} = \sum_{i=1}^{2(n_x+n_c)} w_i \boldsymbol{Y}_i$ $\mathbf{P}_{\boldsymbol{yy}} = \sum_{i=1}^{2(n_x+n_c)} w_i (\boldsymbol{Y}_i - \hat{\boldsymbol{y}})(\boldsymbol{Y}_i - \hat{\boldsymbol{y}})^T + \boldsymbol{R}$ $\mathbf{P}_{\boldsymbol{zy}} = \sum_{i=1}^{2(n_x+n_c)} w_i (\boldsymbol{Z}_i - \hat{\boldsymbol{z}})(\boldsymbol{Y}_i - \hat{\boldsymbol{y}})^T$ $\begin{bmatrix} \mathbf{P}_{\boldsymbol{xy}} \\ \mathbf{P}_{\boldsymbol{cy}} \end{bmatrix} = \mathbf{P}_{\boldsymbol{zy}}$ $\mathbf{K}_{\boldsymbol{z}} = \mathbf{P}_{\boldsymbol{xy}}\mathbf{P}_{\boldsymbol{yy}}^{-1} = \begin{bmatrix} \mathbf{K}_{\boldsymbol{x}} \\ \mathbf{K}_{\boldsymbol{c}} \end{bmatrix} \begin{pmatrix} NOTE: \\ \mathbf{K}_{\boldsymbol{c}} \neq 0!! \end{pmatrix}$ Force correction to consider terms to be 0: $\hat{\boldsymbol{z}}^+ = \hat{\boldsymbol{z}}^- + \begin{bmatrix} \mathbf{K}_{\boldsymbol{x}} \\ \mathbf{0} \end{bmatrix} (\boldsymbol{y} - \hat{\boldsymbol{y}})$ $\mathbf{P}_{\boldsymbol{zz}}^+ = \begin{bmatrix} \mathbf{P}_{\boldsymbol{xx}}^- & \mathbf{P}_{\boldsymbol{xc}}^- \\ \mathbf{P}_{\boldsymbol{cx}}^- & \mathbf{P}_{\boldsymbol{cc}}^- \end{bmatrix} - \begin{bmatrix} \mathbf{K}_{\boldsymbol{x}}\mathbf{P}_{\boldsymbol{yy}}\mathbf{K}_{\boldsymbol{x}}^T & \mathbf{K}_{\boldsymbol{x}}\mathbf{P}_{\boldsymbol{yy}}\mathbf{K}_{\boldsymbol{c}}^T \\ \mathbf{K}_{\boldsymbol{c}}\mathbf{P}_{\boldsymbol{yy}}\mathbf{K}_{\boldsymbol{x}}^T & \mathbf{0} \end{bmatrix}$

Table 1. UKF vs. USKF Formulations

Where $X_{i,k}$ and P_k are the state and covariance of the estimated parameters only, and $Z_{i,k}$ and $P_{zz,k}$ are the augmented state and covariance (i.e. both estimated and considered parameters). Notice that the key difference between the filters is that the update to the consider state and covariance terms are forced to be zero, while the consider-estimated parameter cross-covariance term updates are maintained.

3.3.2 Consider Parameter Implementation

Parameters in an estimator can either be ignored, considered or estimated ("ice"). In this application the state consists of satellite position, velocity, facet sizes, attitudes, body rates and mass. In some cases some of these filter parameters may not be "observable," i.e., there is insufficient information in the observations to estimate them. In this case we might "consider" the parameter – that is, account for our knowledge of its uncertainty in the filter estimates and covariance without actually estimating it. The consider implementation of the UKF is presented in [31] and in the formulations given in Table 1.

3.3.3 Fisher Information

The observation information content for the mass estimation problem is being explored to exploit it to enable one to determine when mass may or may not be observable. Likewise, other parameters associated with the estimation of

mass may or may not be observable. This knowledge can be used to determine when one might "consider" a parameter, including mass. Likewise, once a parameter becomes observable, this knowledge can be used to switch a parameter from being considered to estimated. We propose the use of the Fisher Information matrix. The Fisher information in the USKF is computed as a result of the pre-fit sate covariance, $\bar{P}$, the measurement noise matrix R and the state vs. innovations (observation) cross covariance P_{xy}

$$F_{info} = \tilde{H}^T R^{-1} \tilde{H}$$

where

$$\tilde{H} = \left(\bar{P}^{-1} P_{xy}\right)^T$$

This metric can be viewed as a measure of the state information content provided in the observation data [33, 34, 35].

4. CASE STUDY ANALYSES

The data analysis is set up in a case study format to examine the effects of estimating mass with varying conditions, such as different area-to-mass ratios, observable vs unobservable, and consider implementation.
The information that stayed consistent throughout all cases was:

1. Optical site was located at $253.502751°$ East longitude, $34.96311°$ latitude, 1.725 km above sea level.
2. The albedo $a = 0.3$ for every facet because this is a typical value for satellite material.
3. The duration of observations was originally set to 3 days (72 hours) but filtered down for the times the object could not be seen from the optical site whether for lighting conditions or constraints such as magnitude and earth shadow.

The following figures show the results for different applications. The position, velocity, and mass plots are residual plots that are centered around zero because the data is compared to the truth values using the same dynamics and measurement models.

4.1 An operational GEO with low area-to-mass ratio:

The following Fig.'s 6-9 results present an operational GEO object with an area-to-mass ratio of 0.04 m^2/kg and a fixed attitude. It should be noted that the mass converges much more rapidly due to the higher sensitivity of the SRP acceleration resulting from the higher area-to-mass ration. This is reflected in the Fisher information for each of the states, especially the mass, as indicated in Fig. 10.

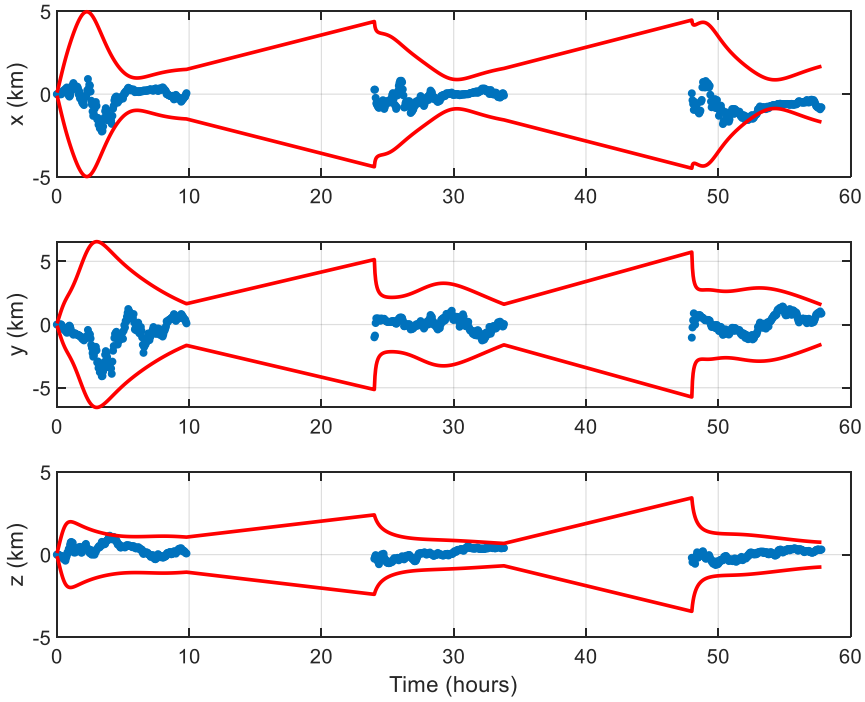

Figure 6. Position Errors and 3σ Bounds

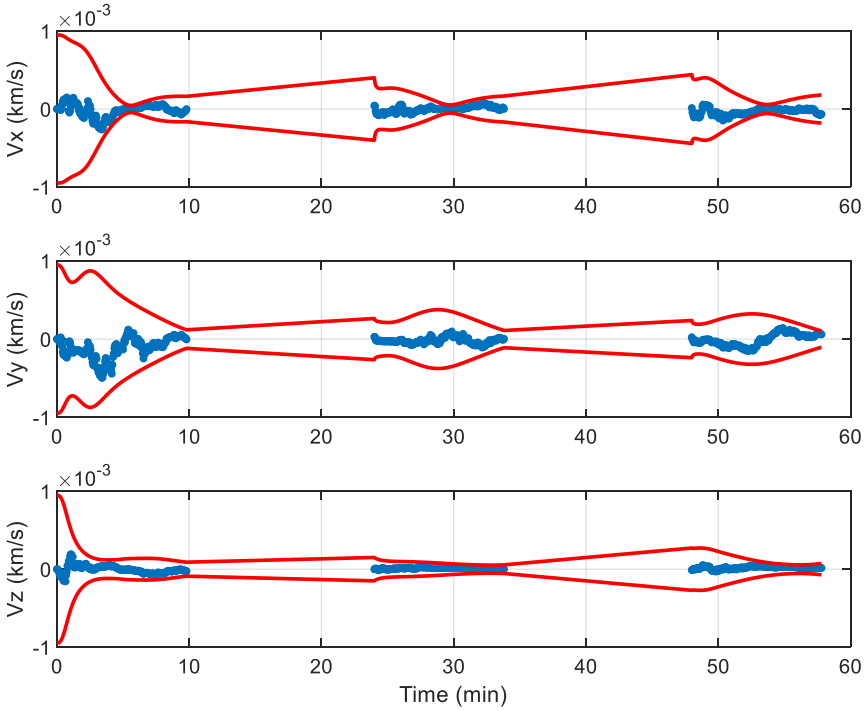

Figure. 7 Velocity Errors and 3σ Bounds

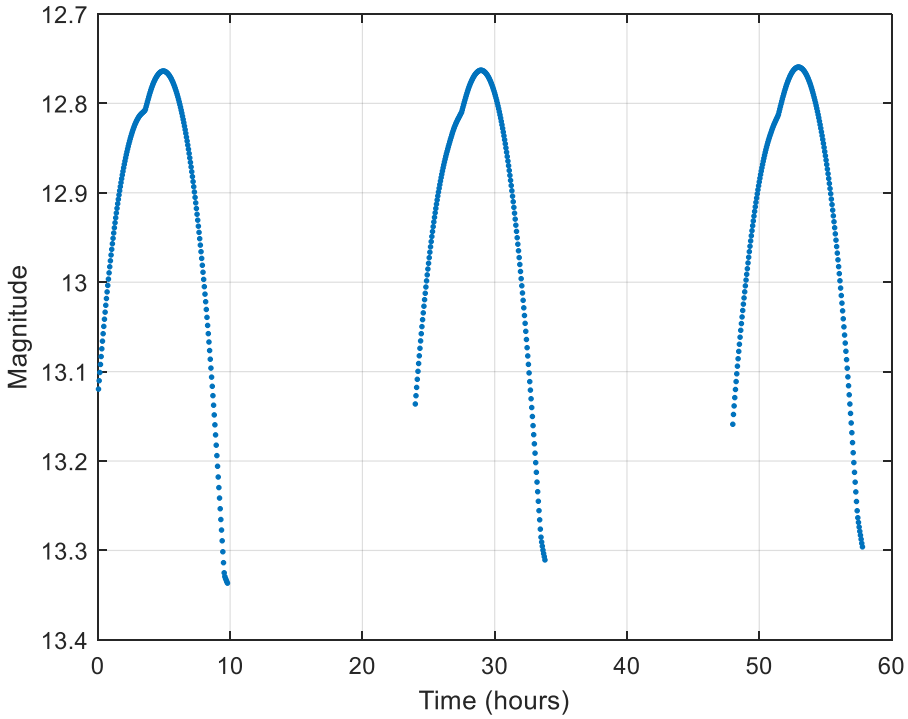

Figure 8. Magnitude

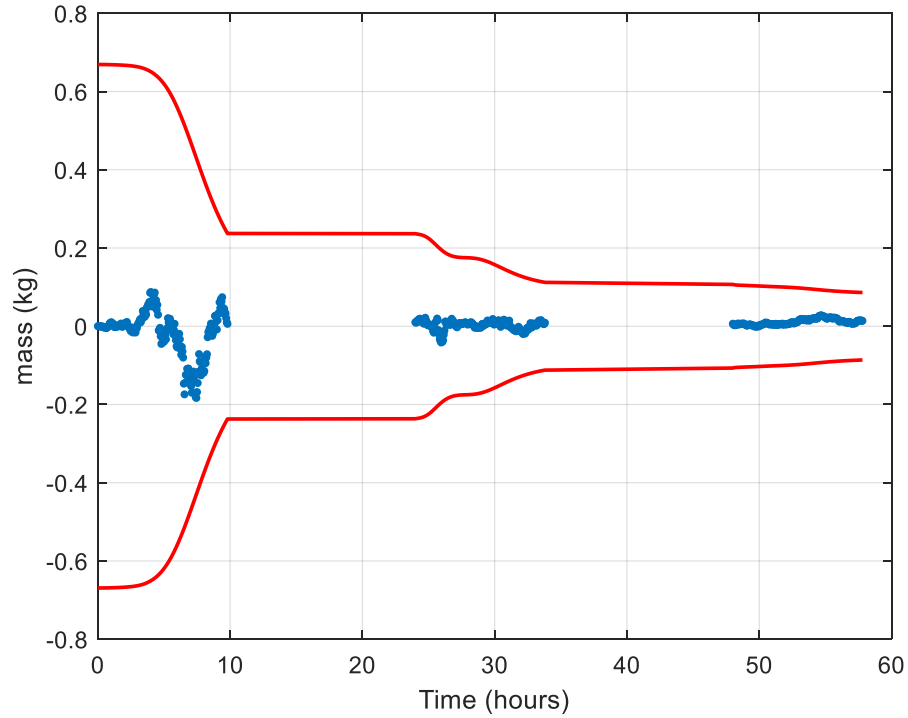

Figure 9. Mass Estimation Errors and 3σ Bounds

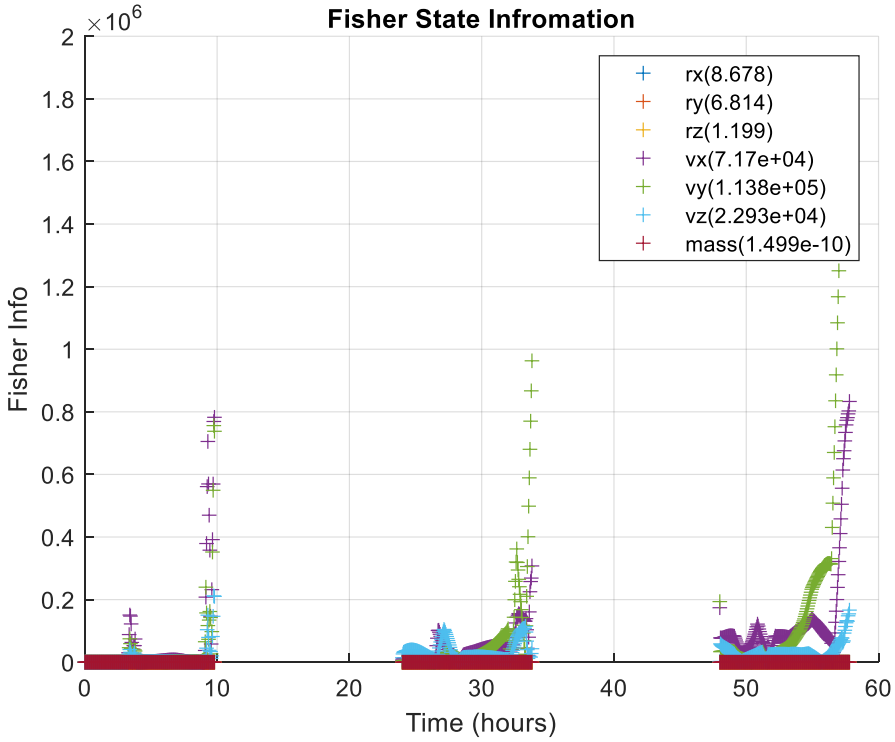

Figure 10. Fisher Information

4.2 A debris GEO with high area-to-mass ratio:

The following results present a HAMR GEO debris object with an area-to-mass ratio of 4.0 m^2/kg and a fixed attitude.

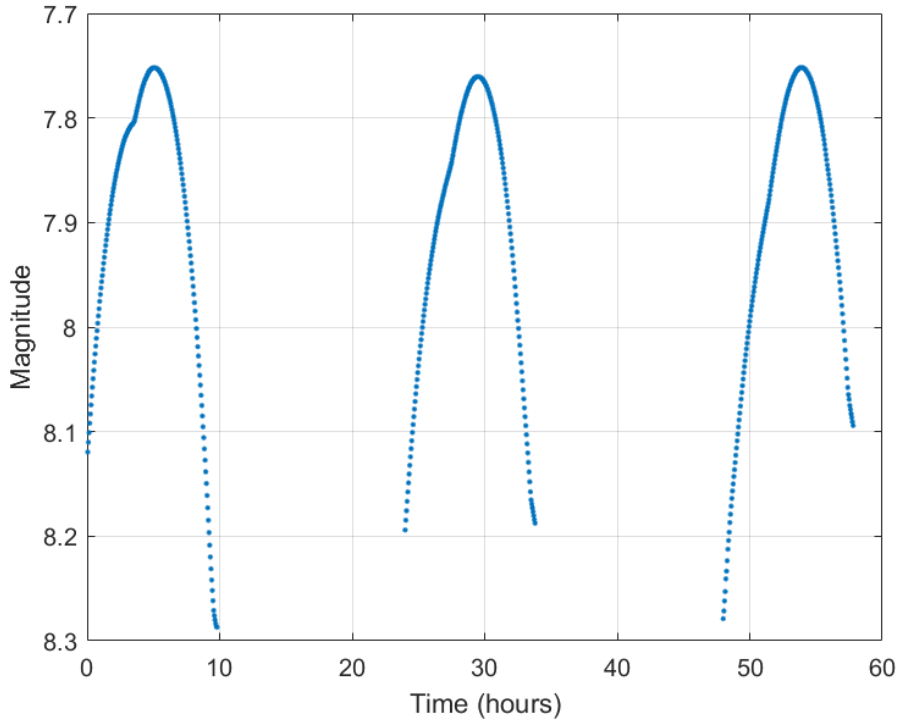

Figure 11. Magnitude

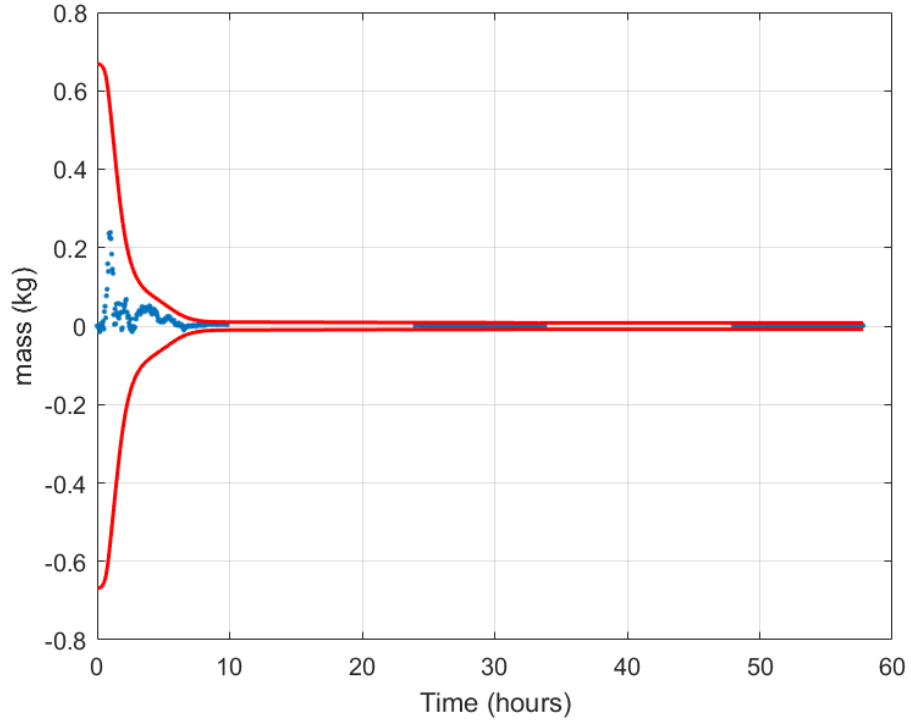

Figure 12. Mass Estimation Errors and 3σ Bounds

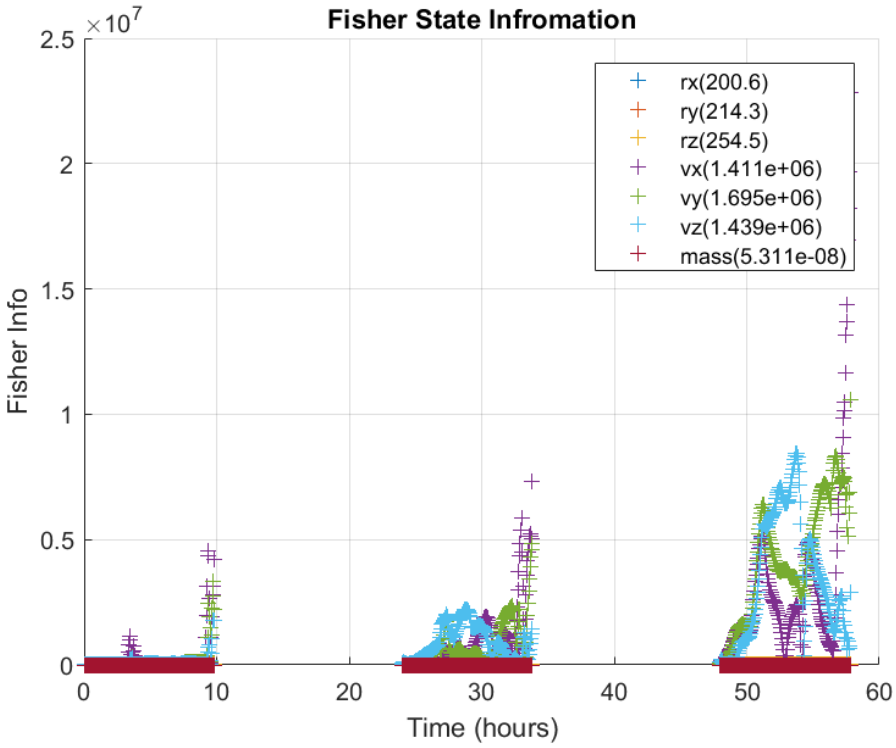

Figure 13. Fisher Information

5. CONCLUSIONS

Several case studies that included attributes for both an operational GEO satellite and a near GEO HAMR debris were examined. The attitude and body rates were initially considered for the 3-axis stabilized, operational GEO case and were estimated for the tumbling "HAMR debris" case. Cases where the size, attitude and mass were observable and where they were not were examined and used to formulate a strategy for estimation vs. consider of state parameters. These techniques were proven to be reliable for representative data quality, cadences and geometries. Future work will further develop the consider vs. estimation implementation in a more automated fashion to base the transition on the observability metric.

It can be seen when comparing at Figures 9 and 12 that the amount of time it takes the filter to converge down to a residual of zero for the mass estimate is significantly different when the object of interest is a HAMR. This can mainly be attributed to the susceptibility of the HAMR to SRP force changes and therefore more information can be gained from the change in dynamics of the object. This is evident in comparing Figures 10 and 13 where the Fisher Information gives insight into the information attainable for each parameter. Since the average information is higher for the mass parameter of the HAMR object we can expect to understand the mass value more accurately as we collect more observations.

6. Future Work

Future work will entail creating a conversion of information in each step of the USKF to a standardized quantity of measurement that can be compared over each step of the filter. This will allow an integration of the Fisher Information with the observability analysis where a parameter will be changed automatically in the filter timestep when enough information has been gained in order to consider a previously unconsidered parameter.

Additional use cases would also prove valuable to know how reliable the filter will be when considering an object that is spinning to see how the mass estimation if affected by a changing attitude where different facets will be seen

for varying amounts of time. Also, more cases where it is known that parameters are not observable will be explored to understand how information changes with the changes in observability.

7. ACKNOWLEDGEMENTS

We would like to thank Dr. Kira Abercrombie at Cal Poly San Luis Obispo for her mentoring and guidance on much of this work presented which was done as part of M. Richardson's MS thesis. We also wish to thank the leadership (Bob MacMillan) at L3 ADS for their encouragement to continue pursuing this line of research towards developing it for "real world" use. Lastly, we want to thank the Air Force Research Laboratory for funding of some elements of the work and continued development.

8. REFERENCES

1 Linares, R., Jah, M.K., Crassidis, J.L., and Neblecky, C.K., 2014. Space Object Shape Characterization and Tracking Using Light Curve and Angles Data, AIAA Journal of Guidance, Control, and Dynamics, Vol. 37, No. 1, Jan.-Feb., pp. 13-25.

2 Wetterer, C. J., Hill, K., and Jah, M. K., 2014. Comparison of Radiation Pressure Perturbations on Rocket Bodies and Debris at Geosynchronous Earth Orbit. The Advanced Maui Optical and Space Surveillance Technologies Conference, Wailea, Maui, Hawaii, September 9-12 (Maui Economic Development Board).

3 Wetterer, C. J., Hunt, B., Kervin, P., and Jah, M. K., 2014. Comparison of Unscented Kalman Filter and Unscented Schmidt Kalman Filter in predicting attitude and associated uncertainty of geosynchronous satellite. The Advanced Maui Optical and Space Surveillance Technologies Conference, Wailea, Maui, Hawaii, September 9-12 (Maui Economic Development Board).

4 Hill, K., Wetterer, C. J., and Jah, M. K. 2014. Comparison of Gravitational, Third-body, and Radiation Pressure Perturbations in Orbit Propagation. 24th AAS/AIAA Spaceflight Mechanics Conference (AAS14-396), Santa Fe, NM, January (American Astronautical Society).

5 Wetterer, C. J., Hunt, B., Hamada, K., Crassidis, J. L., and Kervin, P. 2014. Shape, Surface Parameter, and Attitude Profile Estimation using a Multiple-Hypothesis Unscented Kalman Filter. 24th AAS/AIAA Spaceflight Mechanics Conference (AAS14-303), Santa Fe, NM, January (American Astronautical Society).

6 Wetterer, C. J., Linares, R., Crassidis, J. L., Kelecy, T. M., Ziebart, M. K., Jah, M. K., and Cefola, P. J., "Refining Space Object Radiation Pressure Modeling with Bidirectional Reflectance Distribution Functions," Journal of Guidance, Control, and Dynamics, vol 37: 185-196, 2014.

7 Holzinger, M.J., K. T. Alfriend, C. J. Wetterer, K. Luu, C. Sabol, A. Harms, and K. Hamada, "Attitude Estimation For Agile RSOs With Shape Model Uncertainty Using Lightcurve Inversion and Bayesian Estimation," Journal of Guidance, Control, and Dynamics, 37, 2014.

8 Linares, R., M. K. Jah, J. L. Crassidis, F. A. Leve, T. Kelecy, "Astrometric and Photometric Data Fusion for Space Object Mass and Area Estimation," Acta Astronautica, 99:1,15, 2014.

9 Linares, R., Crassidis, J. L., Wetterer, C. J., Hill, K., and Jah, M. K., "Astrometric and Photometric Data Fusion for Mass and Surface Material Estimation using Refined Bidirectional Reflectance Distribution Functions-Solar Radiation Pressure Model," Advanced Maui Optical and Space Surveillance (AMOS) conference, Wailea, Maui, HI, September 2013.

10 Wetterer, C. J., Crassidis, J. L., Linares, R., Chow, C. C., and Jah, M. K., "Simultaneous Position, Velocity, Attitude, Angular Rates, and Surface Parameter Estimation Using Astrometric and Photometric Observations," Proceedings of the FUSION Conference, Istanbul, Turkey, July 2013.

11 Wetterer, C. J., Linares, R., Crassidis, J. L., Kelecy, T. M., Ziebart, M. K., Jah, M. K., and Cefola, P. J., "Refining Space Object Radiation Pressure Modeling with Bidirectional Reflectance Distribution Functions," 23rd AAS/AIAA Spaceflight Mechanics Conference, Kauai, HI, February 2013.

12 Holzinger, M.J., K. T. Alfriend, C. J. Wetterer, K. Luu, C. Sabol, A. Harms, and K. Hamada, "Attitude Estimation For Agile RSOs With Shape Model Uncertainty Using Lightcurve Inversion and Bayesian Estimation," The Advanced Maui Optical and Space Surveillance Technologies Conference, held in Wailea, Maui, Hawaii, 2012 September 11-14 (Maui Economic Development Board).

13 Linares, R., F. A. Leve, M. K. Jah, J. L. Crassidis, "Space Object Mass-Specific Inertia Matrix Estimation from Photometric Data," 35th Annual AAS Guidance and Control Conference, Breckenridge, CO, February 3-8, 2012.

14 Linares, R., M. K. Jah, J. L. Crassidis, “Inactive Space Object Shape Estimation via Astrometric and Photometric Data Fusion,” 22nd AAS/AAIA Spaceflight Mechanics Meeting, Charleston, SC, January 29 – February 2, 2012.
15 Linares, R., M. K. Jah, J. L. Crassidis, “Space Object Area-to-Mass Ratio Estimation using Multiple Model Approaches,” 35th Annual AAS Guidance and Control Conference, Breckenridge, CO, February 3-8, 2012.
16 Linares, R., M. K. Jah, J. L. Crassidis, F. A. Leve, T. Kelecy, “Astrometric and Photometric Data Fusion for Inactive Space Object Feature Estimation,” 62nd International Astronautical Congress, Cape Town, South Africa, 3-7 October 2011.
17 Harms, A., K. Hamada, C.J. Wetterer, K. Luu, C. Sabol, K.T. Alfriend, “Understanding Satellite Characterization Knowledge Gained from Radiometric Data,” Advanced Maui Optical and Space Surveillance (AMOS) conference, Wailea, HI, September 2011.
18 Linares, R., Crassidis, J. L., Jah, M., and Kim, H., “Astrometric and Photometric Data Fusion for Orbit, Attitude, and Shape Estimation,” AIAA Guidance, Navigation and Control Conference, Chicago, IL, Aug. 2010, AIAA-2009-6293.
19 Wetterer, C.J. and M. K. Jah, “Attitude estimation from light curves,” Journal of Guidance, Control, and Dynamics 32: 1648-1651, 2009.
20 Wetterer, C. J., and M. K. Jah, “Using the Unscented Kalman Filter for Attitude Determination from Light Curves,” 19th AAS/AIAA Spaceflight Mechanics Meeting, Savannah, Georgia, February 2009.
21 M. Jah and R. A. Madler 2007. Satellite characterization: angles and light curve data fusion for spacecraft state and parameter estimation. In Proceedings of the Advanced Maui Optical and Space Surveillance Technologies Conference, volume 49.
22 Chow, Channing, Jack Wetterer, Micah Dilley, Jason Stauch and Jason Baldwin, The Infinity Filter, IAI-PDS white paper, September 1, 2017.
23 D. A. Vallado and W. D. McClain. Fundamentals of Astrodynamics and Applications, The Space Technology Library. Microcosm Press, fourth edition, 2013.
24 R. Linares, M. K. Jah, J. L. Crassidis, F. A. Leve, and T. Kelecy. Astrometric and photometric data fusion for inactive space object mass and area estimation. Acta Astronautica, 99:1–15, 2014.
25 M. Ashikhmin and P. Shirley. An anisotropic phong brdf model. Journal of graphics tools, 5(2):25–32, 2000.
26 H. D. Curtis. Orbital Mechanics for Engineering Students. Elsevier Aerospace Engineering Series. Elsevier, second edition, 2010.
27 T. Kelecy and M. Jah. Analysis of high area-to-mass ratio (hamr) geo space object orbit determination and prediction performance: Initial strategies to recover and predict hamr geo trajectories with no a priori information. Acta Astronautica, 69(7):551–558, 2011.
28 K. J. DeMars. Flat plate and spherical object srp model equivalence. Acquired from Thomas M. Kelecy, August 2011.
29 M. Kaasalainen and J. Torppa. Optimization methods for asteroid lightcurve inversion: I. shape determination. Icarus, 153(1):24–36, 2001. 50
30 B. K. Bradley and P. Axelrad. Improved estimation of orbits and physical properties of objects in geo. In Advanced Maui Optical and Space Surveillance Technologies Conference (AMOS), Maui, HI, 2013
31 J. Stauch and M. Jah, On the Unscented Schmidt-Kalman Filter Algorithm. Journal of Guidance, Control, and Dynamics 38(1): 117-123, 2014.
32 C. Chow, J. Wetterer, M. Dilley, J. Stauch, and J. Baldwin, The Infinity Filter, White Paper, Air Force Research Lab, unpublished.
33 X. Ning, F. Wang, and J. Fang, Implicit UKF and its observability analysis of satellite stellar refraction navigation system, Aerospace Science and Tachnology 54 (2016) 49-58.
34 G. P. Huang and S. I. Roumeliotis, An observability constrained UKF for improving SLAM consistency, Multiple Autonomous Robotic Systems Laboratory technical report number 2008-0002, August 2008.
35 S. M. Baker, C. H. Poskar, and B. H. Junker, Unscented Kalman filter with parameter identifiability analysis for the estimation of multiple parameters in kinetic models, EURASIP Journal on Bioinformatics and Systems Biology 2011.